Nicolae Lobontiu

Jeffrey S. N. Paine

Dynamic Structures and Materials,
LLC 205 Williamson Square,
Franklin, TN 37064

Ephrahim Garcia

Michael Goldfarb

Center for Intelligent Mechatronics,
Vanderbilt University,
Nashville, TN 37235

Corner-Filleted Flexure Hinges

The paper presents an analytical approach to corner-filleted flexure hinges. Closed- form solutions are derived for the in-plane compliance factors. It is demonstrated that the corner-filleted flexure hinge spans a domain delimited by the simple beam and the right circular flexure hinge. A comparison that is made with the right circular flexure hinges indicates that the corner-filleted flexures are more bending-compliant and induce lower stresses but are less precise in rotation. The finite element simulation and experimental results confirmed the model predictions. [DOI: 10.1115/1.1372190]

1 Introduction

The flexure hinge is a mechanical member that substitutes a conventional rotational joint in order to produce a limited angular motion about one axis. Being monolithic with the links it connects, the flexure hinge is highly energy-efficient since it has zero friction and backlash.

A monolithic flexure hinge is usually obtained by machining one or two cutouts in a blank material. In order to be functionally effective, a flexure hinge must be compliant in bending about one axis, to favor the intended rotation, but rigid about the cross axes to prohibit or minimize any other motion. A generic flexure hinge configuration is shown in Fig. 1.

Flexures can be fabricated in several configurations, depending on the cross-section profile. Some of the most common flexure hinges are illustrated in Fig. 2.

The seminal work of Paros and Weisbord [1] constitutes the landmark into the analytical approach of monolithic flexure hinges. The design equations, both exact and simplified, are derived for calculating the compliances (spring rates) of single-axis and two-axes circular-cutout constant cross-section flexure hinges. Specifically, the angular and linear deflections produced on all three axes are expressed in terms of the corresponding external loading.

Ragulskis et al. [2] applied the static finite element analysis to filleted flexure hinges in order to calculate their compliances. The analysis results allowed specifying flexure configurations with minimum bending stiffness.

In an approach similar to that of Paros and Weisbord [1], Smith et al. [3] provided closed- form equations for the mechanical compliance of elliptic cross-section flexure hinges. An elliptical flexure hinge is ranging between a circular flexure hinge and a simple beam in term of its compliance. The model accuracy was verified by finite element analysis and experimental measurements.

Xu and King [4] performed static finite element analysis of corner-filleted and elliptic flexure hinges. A comparison was made with right circular flexure hinges which revealed that the corner-filleted flexure is the most accurate in terms of motion, the elliptic flexure has less stress for the same displacement, while the right circular flexure is the stiffest.

There are several papers presenting applications that incorporate flexure hinges into specific designs. A few are mentioned in the following.

Weinstein [5] introduced the single-, two- and three-strip flexure pivot bearings. The beam theory was used to analyze design issues by means of equations giving the spring rate and several dimensionless-parameter diagrams.

Goldfarb and Speich [6] presented the design and analysis of a revolute joint for compliant mechanisms consisting of a longitudinally-split thin cylinder.

Lobontiu [7] analyzed the dynamic response of a two-link pendulum with rectangular flexure hinges that are substantially thinner than the adjoining links. Designs were proposed in terms of the defining geometry that would enable the free extremity follow a prescribed trajectory.

Her and Chang [8] proposed an analytical scheme that allows displacement calculations for micro-positioning stages with integrated flexure hinges. The method was assessed by comparison to finite element results.

Howell and Midha [9] introduced a computer-aided design approach to pseudo-rigid-body mechanisms that include compliant flexure pivots. The corresponding analysis consists of a rigid-body kinematic module coupled with a finite element-type large deflection algorithm dedicated to the short flexure hinges.

Ryu, Gweon, and Moon [10] developed the mathematical model of a three degree-of- freedom micro-motion stage that incorporates several right circular flexure hinges and levers. An equivalent mass-spring system was further analyzed, and force-displacement equations were formulated enabling to maximize the amplification of the micro-stage under specified restrictions.

Ryu and Gweon [11] proposed a modeling and quantifying scheme of the motion errors induced by machining imperfections into a flexure hinge mechanism.

Ryu et al. [12] analyzed a flexure hinge mechanism consisting of levers (modeled as rigid bodies), flexure hinges, and piezoelec-

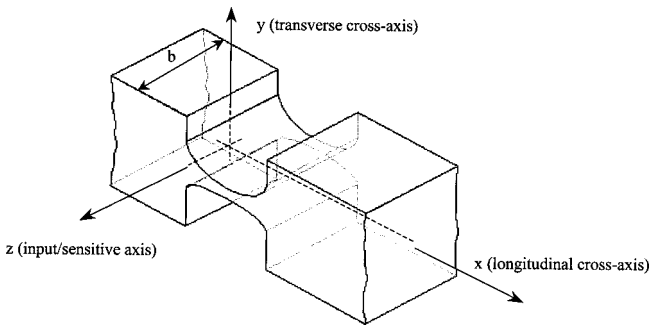

Fig. 1 Geometry and reference axes of a generic constant-width flexure hinge

Contributed by the Reliability Stress Analysis & Failure Prev. Committee for publication in the JOURNAL OF MECHANICAL DESIGN. Manuscript received Oct. 2000. Associate Editor: J. Gao.

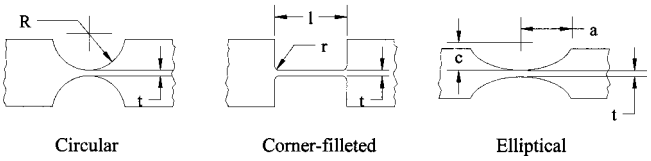

Fig. 2 Representative flexure hinges with main geometric parameters

tric actuators (modeled as rotational/translational springs). The inverse kinematic model yields the input voltage – output displacement relationship.

This paper addresses the corner-filleted flexure hinges. Their in-plane behavior is only analyzed since these rotational connectors are designed to be incorporated in planar mechanisms. The closed-form compliance factors are formulated in terms of length *l*, thickness *t* and fillet radius *r* for constant-width, corner-filleted flexure hinges. It is demonstrated that a corner-filleted flexure hinge spans a domain bounded by the simple beam ($r = 0$) and the right circular flexure hinge ($r = l/2$). Finite element simulations are performed to verify the accuracy of the model-predicted compliance factors for several design configurations. The results are in good agreement with those produced by the analytical approach within 10 percent relative error margins. The experimental measurements also confirm the analytical predictions with relative errors less than 6 percent. Compared to the right circular flexures, the corner-filleted flexures can be up to 6 times more bending-compliant. They also induce substantially lower stresses but are less precise in keeping the position of the rotation center. All these conclusions are formulated by analyzing several ratio functions that are defined in terms of two non-dimensional variables.

2 Motivation and Assumptions

The authors are implementing corner-filleted flexure hinges into piezoelectric-driven amplification mechanisms. A typical configuration is sketched in Fig. 3 that can amplify the input displacement more than 20 times in an optimized design while Fig. 4 shows the geometry of a generic corner-filleted flexure hinge.

The paper characterizes the corner-filleted flexure hinges in terms of compliance to external loading, precision of rotation and stress levels by providing closed-form solutions to these problems as efficient alternatives to the more time-consuming finite element approach.

The mathematical model is based on several simplifying assumptions that are summarized in the following:

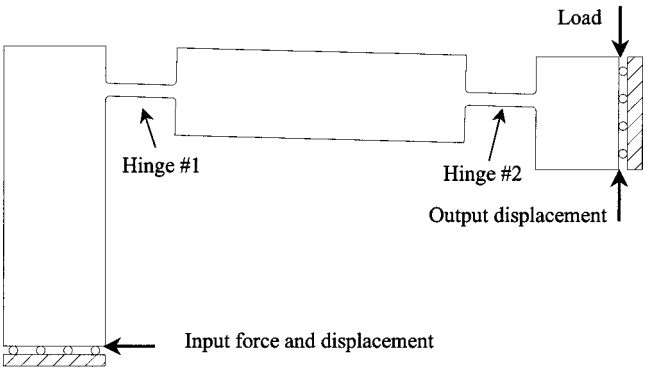

Fig. 3 Quarter-model of a 2D amplification mechanism; hinge #1 is subject to bending (from input and loading), tension (from input) and shearing (from loading)

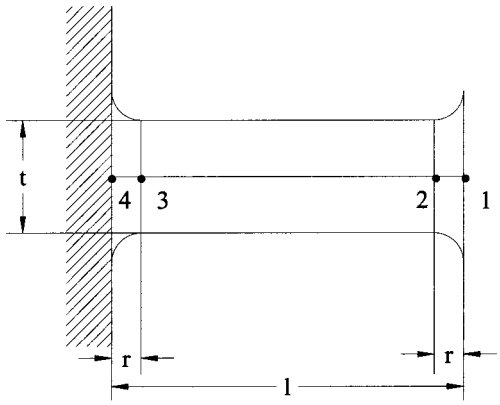

Fig. 4 Geometry of a corner-filleted flexure hinge

• The flexure hinges are assumed to be long and thus, according to strength of materials (see Young [13], for instance), the deflection due to shearing is negligible for such beam-like structures.

• The hinges discussed here are part of plane devices where both the input and output are planar; essentially this allows conducting the study for only three degrees of freedom: two in-plane translations and one rotation, normal to the translation plane.

• Compared to other effects, the bending and axial tension/compression are prevalent and thus only these factors are considered in all subsequent derivation.

• Since all deformations of a flexure hinge are small, the small displacement theory is applied for both bending and axial effects.

• The boundary conditions for a flexure hinge are fixed-free, and this is a good approximation provided the loading is accurately specified.

• The beam comprises three portions: two are mirrored-identical and have variable cross-sections at the filleted ends, while the middle segment is of constant cross-section.

• The Castigliano's second theorem is utilized throughout this paper to formulate the compliances of corner-filleted flexure hinges.

3 Compliance Model

3.1 Problem Formulation. Figure 5 indicates the loading and deformations of a beam-like corner-filleted flexure hinge.

The Castigliano's first theorem is applied in order to express the displacements at the flexure's free end:

$$\begin{cases} \theta_1 = \dfrac{\partial U_e}{\partial M_{z1}} \\ y_1 = \dfrac{\partial U_e}{\partial F_{y1}} \\ x_1 = \dfrac{\partial U_e}{\partial F_{x1}} \end{cases} \tag{1}$$

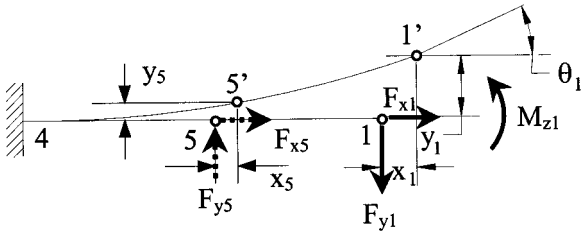

Fig. 5 Schematic showing deformations at the free end and displacement of the theoretical rotation center

where the elastic strain energy is:

$$U_e = 1/2\left[\int_L M^2/(EI)ds + \int_L N^2/(EA)ds\right] \tag{2}$$

The equations providing the moment of area, bending moment M and axial force N over different intervals are given in the Appendix. Equations (1) and (2) result in:

$$\begin{Bmatrix} \theta_1 \\ y_1 \\ x_1 \end{Bmatrix} = \begin{bmatrix} C_{11} & C_{12} & 0 \\ C_{12} & C_{22} & 0 \\ 0 & 0 & C_{33} \end{bmatrix} \begin{Bmatrix} M_{z1} \\ F_{y1} \\ F_{x1} \end{Bmatrix} \tag{3}$$

where the compliances are:

$$\begin{cases} C_{11} = 3/(bE)[1/2(I_1+I_3)+4(l-2r)t^{-3}] \\ C_{12} = -3/(bE)[1/2(I_2+I_4)+2l(l-2r)t^{-3}] \\ C_{22} = 3/(bE)[1/2(I_5+I_6)+4/3(l-2r)(l^2-lr+r^2)t^{-3}] \\ C_{33} = 1/(bE)[1/2(I_7+I_8)+(l-2r)t^{-1}] \end{cases} \tag{4}$$

The I_1 through I_8 integrals are:

$$I_1 = \int_0^r dx/A(x)^3 \tag{5}$$

$$I_2 = \int_0^r x\,dx/A(x)^3 \tag{6}$$

$$I_3 = \int_r^{l-r} dx/B(x)^3 \tag{7}$$

$$I_4 = \int_r^{l-r} x\,dx/B(x)^3 \tag{8}$$

$$I_5 = \int_0^r x^2 dx/A(x)^3 \tag{9}$$

$$I_6 = \int_r^{l-r} x^2 dx/B(x)^3 \tag{10}$$

$$I_7 = \int_0^r dx/A(x) \tag{11}$$

$$I_8 = \int_r^{l-r} dx/B(x) \tag{12}$$

with:

$$A(x) = t/2 + r - \sqrt{x(2r-x)} \tag{13}$$

$$B(x) = t/2 + r - \sqrt{(l-x)[2r-(l-x)]} \tag{14}$$

Equations (4) through (14) produce the closed-form compliance factors:

$$\begin{aligned} C_{11} = {} & 12/(Ebt^3)\{l-2r+2r[t(4r+t)(6r^2+4rt+t^2) \\ & +6r(2r+t)^2 t^{1/2}(4r+t)^{1/2} a\tan(1+4r/t)^{1/2} \\ & \times(2r+t)^{-1}(4r+t)^{-3}\} \end{aligned} \tag{15}$$

$$\begin{aligned} C_{12} = {} & -6l/[Ebt^3(2r+t)(4r+t)^2][l(2r+t)(4r+t)^2 \\ & -4r^2(16r^2+13rt+3t^2)+12r^2(2r+t)t^{1/2}(4r+t)^{1/2} \\ & \times a\tan(1+4r/t)^{1/2}] \end{aligned} \tag{16}$$

$$\begin{aligned} C_{22} = {} & 3/(Eb)\{4(l-2r)(l^2-lr+r^2)/(3t^3)^{-1} \\ & +1/2\{\{t^{1/2}(4r+t)^{1/2}[-80r^4+24r^3t+8(3+2\pi)r^2t^2 \\ & +4(1+2\pi)rt^3+\pi t^4]+4(2r+t)^3(6r^2-4rt-t^2) \\ & \times a\tan(1+4r/t)^{1/2}\}/[2t^{5/2}(4r+t)^{5/2}]^{-1} \\ & +[-40r^4+8lr^2(2r-t)+12r^3t+4(3+2\pi)r^2t^2 \\ & +2(1+2\pi)rt^3+\pi t^4/2]/t^{-2}(4r+t)^{-2} \\ & +8l^2r(6r^2+4rt+t^2)(2r+t)^{-1}t^{-2}(4r+t)^{-2} \\ & -\{2(2r+t)[-24(l-r)^2r^2-8r^3t+14r^2t^2+8rt^3+t^4] \\ & \times a\tan(1+4r/t)^{1/2}]t^{-1/2}(4r+t)^{-1/2}t^{-2}(4r+t)^{-2}\}\} \end{aligned} \tag{17}$$

$$\begin{aligned} C_{33} = {} & 1/(Eb)[-\pi/2+(l-2r)/t+2(2r+t)t^{-1/2}(4r+t)^{-1/2} \\ & \times a\tan(1+4r/t)^{1/2}] \end{aligned} \tag{18}$$

3.2 Limits to the Compliance Factors. The fillet radius r can only vary between $r_{min}=0$ (when the flexure is actually a simple beam) and $r_{max}=l/2$ (when the corner-filleted flexure becomes a right circular flexure).

In both cases, expressions are available for the compliance factors from the engineering theory of beams and the work of Paros and Weisbord [1] that treated the problem of circular flexure hinges.

It is demonstrated in the following that the compliance expressions of a generic corner-filleted flexure match their aforementioned limits.

(a) Non-filleted flexure ($r = 0$; engineering beam theory)

Taking $r = 0$ in Eq. (15) gives:

$$C_{11} = 12l/(Ebt^3) \tag{19}$$

Equation (19) is identical to the beam theory formula that expresses the end rotation produced by an end bending moment for a fixed-free beam.

Taking $r = 0$ in Eq. (16) produces:

$$C_{12} = -6l^2/(Ebt^3) \tag{20}$$

which is identical to the solution given by the beam theory that relates the end deflection to the end bending moment for a fixed-free beam.

Taking $r = 0$ in Eq. (17) yields:

$$C_{22} = 4l^3/(Ebt^3) \tag{21}$$

which coincides with the simple beam formula that assesses the end deflection determined by an end force for a fixed-free beam.

Taking $r = 0$ in Eq. (18) gives:

$$C_{33} = l/(Ebt) \tag{22}$$

which is the same as given by theory for a simple fixed-free bar in extension.

(b) Right circular flexure ($r = l/2$; compliances given in Paros and Weisbord [1])

Using the notations that were introduced by Paros and Weisbord [1], namely:

$$\beta = t/(2r) \tag{23}$$

and

$$\gamma = h/(2r) \tag{24}$$

where:

$$h = 2r + t \tag{25}$$

and substituting them into Eq. (15) yields:

$$C_{11}=3/[2Ebr^2\beta(\beta+2)]\{1/(\beta+1)+(3+2\beta+\beta^2)/[\beta(\beta+1)(\beta+2)]+6(\beta+1)\times\beta^{-3/2}(\beta+2)^{-3/2}a\tan(1+2/\beta)^{1/2}\} \quad (26)$$

which is identical to what Eq. (1) of Paros and Weisbord [1] produces by taking:

$$\gamma=\beta+1 \quad (27)$$

Similarly, Eq. (16) transforms into:

$$C_{12}=rC_{11} \quad (28)$$

which is identical to Eq. (3) of Paros and Weisbord [1] in the particular case of right circular flexures.

Equation (17) can be reformulated as:

$$C_{22}=3/[2Eb\beta^3(1+\beta)(2+\beta)^3]\{\beta(2+\beta)\times[3+6\beta+(11+4\pi)\beta^2+8(1+\pi)\beta^3+(2+5\pi)\beta^4+\pi\beta^5]-2(1+\beta)^4\times\beta^{1/2}(2+\beta)^{1/2}(-3+4\beta+2\beta^2)a\tan(1+2/\beta)^{1/2}\} \quad (29)$$

and this is identical to Eq. (9) of Paros and Weisbord [1] for right circular flexures.

Equation (18) gives:

$$C_{33}=1/(Eb)[-\pi/2+2(1+\beta)\beta^{-1/2}(\beta+2)^{-1/2}a\tan(1+2/\beta)^{1/2}] \quad (30)$$

which coincides to what Eq. (25) of Paros and Weisbord [1] yields for right circular flexures.

3.3 Corner-Filleted Versus Right Circular Flexure Hinges in Terms of Compliance. A comparison is performed between corner-filleted and right circular flexures in terms of their compliances. The following non-dimensional variables are introduced:

$$\begin{cases}\delta=t/l\\ \varepsilon=r/l\end{cases} \quad (31)$$

The non-dimensional variables defined in Eq. (31) are now used to compare the corner- filleted flexure hinges to their corresponding equal-length, right circular flexure hinges in terms of compliances. The (*) superscript indicates a right circular flexure hinge and the (*) compliances are obtained by taking $l = 2r$.

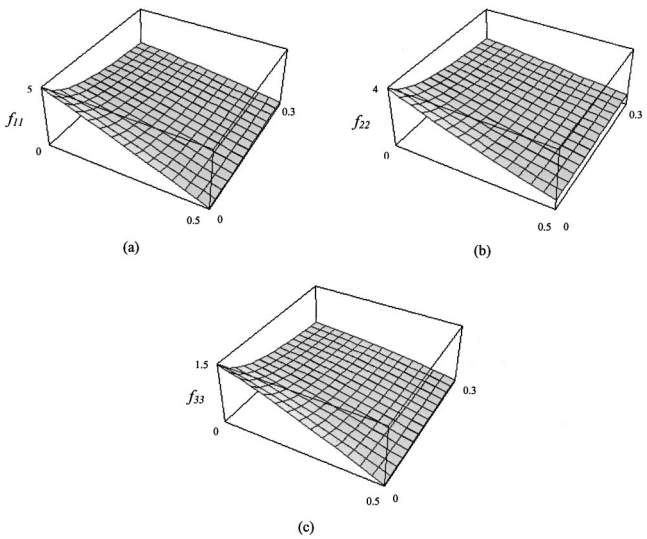

Fig. 6 Plot of non-dimensional compliance ratios: (*a*) $f_{11}=C_{11}/C_{11}^*$; (*b*) $f_{22}=C_{22}/C_{22}^*$; (c) $f_{33}=C_{33}/C_{33}^*$

Specifically, three functions are defined in the following. The first function is:

$$f_{11}(\delta,\varepsilon)=C_{11}/C_{11}^* \quad (32)$$

where C_{11} and C_{11}^*, are simply obtained from Eq. (15) by using the notations given in Eq. (31). It also can be seen that:

$$C_{12}/C_{12}^*=f_{11}(\delta,\varepsilon) \quad (33)$$

where C_{12} and C_{12}^*, are given by Eqs. (16) and (31).

The next function is:

$$f_{22}(\delta,\varepsilon)=C_{22}/C_{22}^* \quad (34)$$

where C_{22} and C_{22}^*, are simply obtained from Eq. (17) by using the notations given in Eq. (31). The last function is:

$$f_{33}(\delta,\varepsilon)=C_{33}/C_{33}^* \quad (35)$$

with C_{33} and C_{33}^*, yielded by Eqs. (18) and (31).

Figures 6(*a*), 6(*b*) and 6(*c*) are three-dimensional plots of the functions defined above.

The corner-filleted flexure hinge can be 5 to 6 times more bending-sensitive compared to its right circular counterpart, when the fillet radius is sufficiently small, as illustrated in Figs. 6(*a*) and 6(*b*). At the same time though, a corner-filleted flexure hinge is more axially-sensitive at small fillet radii than its corresponding right circular flexure (up to 1.5 times, as indicated in Fig. 6(*c*)).

4 Precision of Rotation

4.1 Problem Formulation. Ideally, the center of the flexure, which can also be considered as the 'center of rotation,' (point 5 in Fig. 5), should not translate at all under the loading, but this is actually impossible since the whole flexure deforms under the combined action of bending and tension.

In order to quantify the offset of the center of rotation, the horizontal and vertical displacements x_5 and y_5 are calculated by superimposing two 'dummy' loads F_{x5} and F_{y5} to the actual loads F_{x1}, F_{y1} and M_{z1} (see Fig. 5). The Castigliano's first theorem is subsequently applied in the form:

$$\begin{cases}y_5=\dfrac{\delta U_e}{\delta F_{y5}}\\ x_5=\dfrac{\delta U_e}{\delta F_{x5}}\end{cases} \quad (36)$$

where U_e is given in Eq. (2). The bending moment M and axial force N are provided in the Appendix.

The displacement of the center of rotation can be alternatively expressed in matrix form as:

$$\begin{Bmatrix}0\\ y_5\\ x_5\end{Bmatrix}=\begin{bmatrix}0 & 0 & 0\\ C'_{12} & C'_{22} & 0\\ 0 & 0 & C'_{33}\end{bmatrix}\begin{Bmatrix}M_{z1}\\ F_{y1}\\ F_{x1}\end{Bmatrix} \quad (37)$$

with:

$$\begin{cases}C'_{12}=(3/2bE)[(l-2r)^2t^{-3}+I_4-l/2I_3]\\ C'_{22}=-3/(bE)\{(3t^3)^{-1}[(l-r)^2(l-4r)+l^3/4]+1/2(I_6-l/2I_4)\}\\ C'_{33}=1/2C_{33}\end{cases} \quad (38)$$

The integrals I_3, I_4 and I_6 are defined in Eqs. (7), (8), (10) while C_{33} is given in Eq. (18).

The closed-form solutions for C'_{12} and C'_{22} are:

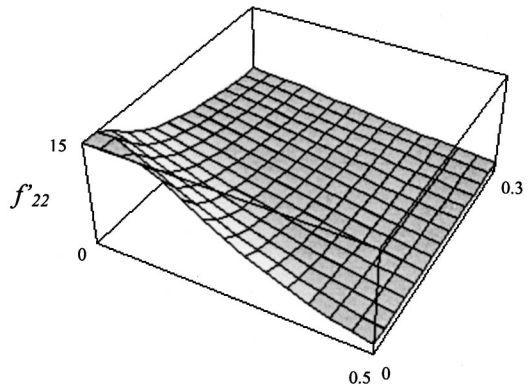

Fig. 7 Plot of non-dimensional compliance ratio $f'_{22}=C'_{22}/C^{*\prime}_{22}$

$$C'_{12}=3/[2bt^3(2r+t)(4r+t)^{5/2}E]\{(4r+t)^{1/2}[l^2(2r+t)(4r+t)^2+8r^3(2r+t)(8r+5t)-8lr^2(16r^2+13rt+3t^2)]+24(l-2r)r^2(t)^{1/2}(2r+t)^2a\tan(1+4r/t)^{1/2}\} \quad (39)$$

$$C'_{22}=1/[4bt^3(2r+t)(4r+t)^{5/2}E]\{(4r+t)^{1/2}\{-5l^3(2r+t)(4r+t)^2-72lr^3(2r+t)(8r+5t)+48l^2r^2(16r^2+13rt+3t^2)+(2r+t)[256r^5+368r^4t-56r^3t^3-24(3+2\pi)r^2t^3-12(1+2\pi)rt^4-3\pi t^5)]\}+12(t)^{1/2}(2r+t)^2[-12l^2r^2+36lr^3-(2r+t)^2(6r^2-4rt-t^2)]a\tan(1+4r/t)^{1/2}\} \quad (40)$$

4.2 Corner-Filleted Versus Right Circular Flexure Hinges in Terms of Precision of Rotation. The corner-filleted flexure hinges are now compared to the corresponding equal-length right circular flexure hinges in terms of their precision of rotation as described by Eqs. (39) and (40). The non-dimensional variables δ and ε introduced in Eq. (31) are used to define the following functions:

$$f'_{12}(\delta,\varepsilon)=C'_{12}/C^{*\prime}_{12} \quad (41)$$

$$f'_{22}(\delta,\varepsilon)=C'_{22}/C^{*\prime}_{22} \quad (42)$$

The expressions of $C^{*\prime}_{12}$ and $C^{*\prime}_{22}$ are simply obtained from Eqs. (39) and (40) by taking $l=2r$. Figure 7, for instance, shows the three-dimensional plot of the f'_{22} function defined above.

As a consequence of being more compliant than the right circular flexure hinges, the corner-filleted flexures are also less precise in keeping the center of rotation with minimum offset. The shift of the rotation center caused by bending effects only can be 10 to 15 times larger in a corner-filleted flexure than the shift experienced by a similar right circular flexure hinge for the same amount of loading. For small/micro-scale applications where two links connected by a flexure must replicate pure rotation as close as possible, this aspect might pose serious limitations. In medium/macro-scale applications though, this relative disadvantage is not paramount since the gains of large motion capability at lower stress levels are strong factors in favor of the corner-filleted flexure. It is also worth noting that Fig. 7 depicts the relationship between the two flexure types in a relative fashion. In reality, the absolute values of the rotation center's shift are very small, and they do not seriously endanger the precision of the relative rotation between two adjoining links.

5 Stress Limitations

5.1 Problem Formulation. The normal stresses on the cross-section of the flexure hinge are the result of bending and axial loading when shearing, as previously stated, is neglected. The filleted area can be looked at as a stress concentrator. As a result, the maximum stress on the upper fiber can be expressed as:

$$\sigma_{\max}=6k_b(M_{z1}+F_{y1}l)/(bt^2)+k_aF_{x1}/(bt) \quad (43)$$

assuming that both M_{z1} and F_{y1} have similar bending effects. The stress concentration factors k_b (in bending) and k_a (in axial loading) can be found in textbooks like those of Young [13] or Peterson [14]. Equation (43) is useful when the external loads acting on the flexure are known in advance. Often times, though, the loading is at least partially unknown, but the displacement field is specified and, as a consequence, Eq. (43) needs to be modified accordingly. Equation (3) is first expressed as:

$$\begin{Bmatrix} M_{z1} \\ F_{y1} \\ F_{x1} \end{Bmatrix} = \begin{bmatrix} K_{11} & K_{12} & 0 \\ K_{12} & K_{22} & 0 \\ 0 & 0 & K_{33} \end{bmatrix} \begin{Bmatrix} \theta_1 \\ y_1 \\ x_1 \end{Bmatrix} \quad (44)$$

where the stiffness terms are:

$$\begin{cases} K_{11}=C_{22}/(C_{11}C_{22}-C_{12}^2) \\ K_{12}=-C_{12}/(C_{11}C_{22}-C_{12}^2) \\ K_{22}=C_{11}/(C_{11}C_{22}-C_{12}^2) \\ K_{33}=1/C_{33} \end{cases} \quad (45)$$

Substituting M_{z1}, F_{y1} and F_{x1} from the matrix Eq. (44) into Eq. (43) results in:

$$\sigma_{\max}=6k_b/(bt^2)[(K_{11}+lK_{12})\theta_1+(K_{12}+lK_{22})y_1]+k_a/(bt)K_{33}x_1 \quad (46)$$

Equation (46) allows evaluating the maximum stress in terms of the specified displacement values at the tip of the flexure. Both Eq. (43) and Eq. (46) could be utilized in actually designing or only checking an already-designed corner-filleted flexure. Designing a flexure by means of Eq. (46) would imply multi-dimensional non-linear optimization and this is beyond the scope of the present work.

5.2 Corner-Filleted Versus Right Circular Flexure Hinges in Terms of Stress. The stress concentration factors for both corner-filleted and circular flexure hinges are of the same order of magnitude, and generally less than 3 as indicated by Peterson [14].

The difference in stress levels, if any, between the two flexures is then produced by the stiffness difference, as suggested in Eq. (46).

A comparison is carried out between the stiffness factors. Again, the non-dimensional variables of Eq. (31) are utilized.

The following function is introduced:

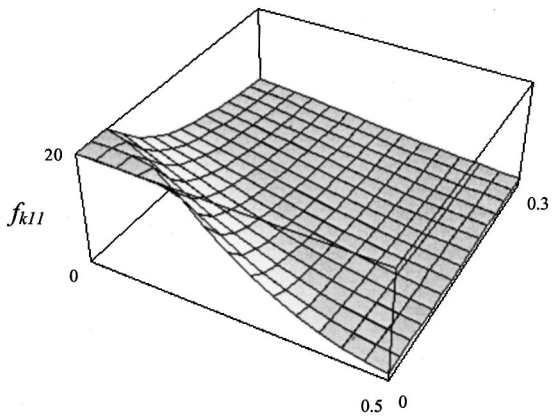

Fig. 8 Plot of non-dimensional stiffness ratio $f_{k11}=K^*_{11}/K_{11}$

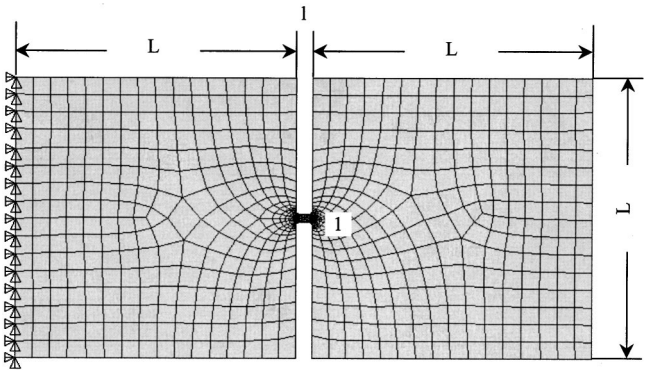

Fig. 9 Finite element model for a corner-filleted flexure hinge

$$f_{k11}(\delta,\varepsilon)=K_{11}^{*}/K_{11} \tag{47}$$

where the superscript denotes the right circular flexure hinge. K_{11}^{*} is simply obtained by taking $l = 2r$ in Eq. (45). Figure 8 shows the three-dimensional plot of this function.

Similar results were obtained for the other stiffness ratios that have been accordingly defined and therefore no other plots are included here.

Figure 8 indicates that the stiffness of a right circular flexure hinge can be 20 times higher than the one of a corresponding corner-filleted flexure hinge with small fillet radii, and this directly translates to the stress levels, as Eq. (46) indicates.

6 Finite Element Results

The finite element model shown in Fig. 9 was utilized to verify the compliance equations for several corner-filleted flexure designs. The ANSYS finite element software was used to run all finite element static-load simulations. Two dimensional, 6 degree-of-freedom per node, Shell 63 elements were utilized. It was considered that the flexures are made of 5×10^{-3} [m] thick titanium alloy with a Young's modulus of 11×10^{10} [Pa] and a Poisson's ratio of 0.33. Vertical forces F_y, horizontal forces F_x, and moments M_z were sequentially applied at point 1 (Figure 9 where $l =$ 0.01 [m]), and the corresponding vertical displacements, horizontal displacements, and rotations were read. This allowed calculation of C_{11}, C_{12}, C_{22} and C_{33} by means of Eq. (3).

Table 1 comprises the analytical and finite element results together with the design parameters of several flexure hinges.

The analytical and numerical data were in good agreement, as Table 1 shows it. The relative errors between analytical and finite element results were less than 10 percent.

7 Experimental Results

Two 5×10^{-3} [m] thick aluminum corner- filleted flexure hinge specimens were fabricated and tested in bending. Two different experimental setups were arranged in order to determine the compliance factors C_{12} and C_{22}. In one test, a couple was applied to the flexure by means of two equal and opposite forces F_x, as sketched in Fig. 10(*a*). The couple consisted of two equal weights that were applied symmetrically with respect to the flexure longitudinal axis. An eddy current displacement sensor was used to measure the deflection at point 1. Knowing the loads and their spacing d, provided the value of the moment M_{z1}. It was thus possible to evaluate the compliance factor C_{12} for each load step, as indicated in Eq. (3). A similar procedure was utilized to evaluate the compliance factor C_{22} by measuring the deflection at point 1 under several weights also applied at 1, as shown in Fig. 10(*b*). The experimental data is summarized in Table 2.

The specimens were loaded with seven different loads in each experimental setup and the corresponding compliances were calculated as average values. The results for a given specimen and test were consistent within a 4 percent error margin. The experimental data confirmed the theoretical model predictions with relative errors less than 6 percent.

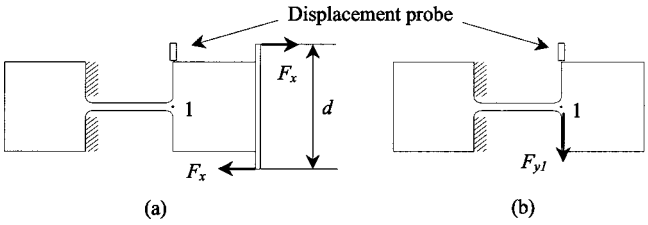

Fig. 10 Schematics of the experiment: (*a*) setup for evaluation of C_{12}; (*b*) setup for evaluation of C_{22}

Table 2 Experimental and analytical compliance data

		Sample # 1	Sample # 2
l [m x 10^{-3}]		25.40	19.05
t [m x 10^{-3}]		2.27	1.44
r [m x 10^{-3}]		3.17	3.17
C_{12} [N^{-1}x10^{-6}]	Experimental	1913	3834
	Analytical	1798	3611
C_{22} [mN^{-1}x10^{-9}]	Experimental	28925	42995
	Analytical	28600	41641

8 Conclusions

The paper presents an analytic approach to corner-filleted flexure hinges that are utilized in monolithic mechanisms to produce limited rotation. The closed-form solutions of the compliance factors for corner-filleted flexure hinges are derived. It is demonstrated that a corner-filleted flexure hinge spans a field whose limits are the simple beam (for a fillet radius of $r = 0$) and the right circular flexure hinge (for a fillet radius of $r = l/2$). The finite element results are in good agreement with those yielded by the analytical approach with relative errors less than 10 percent.

Table 1 Analytical and finite element compliance data

			C_{11} [$N^{-1}m^{-1}$x10^{-3}]		C_{12} [N^{-1}x10^{-6}]		C_{22} [mN^{-1}x10^{-9}]		C_{33} [mN^{-1}x10^{-11}]	
l [mx10^{-3}]	t [mx10^{-3}]	r [mx10^{-3}]	Analytic	FEM	Analytic	FEM	Analytic	FEM	Analytic	FEM
1.6	0.5	0.25	248.995	271.342	199.196	201.160	202.715	204.491	554.110	595.837
1.6	0.5	0.30	239.228	250.167	191.382	199.036	192.118	204.286	543.945	585.891
1.6	0.6	0.25	145.836	152.226	116.669	112.509	119.321	128.373	464.690	508.079
1.6	0.6	0.30	140.590	143.568	112.472	119.192	113.593	123.237	457.718	506.694
1.8	0.5	0.25	283.904	291.081	255.514	231.926	293.847	298.374	626.837	667.336
1.8	0.5	0.30	274.137	260.476	246.723	253.395	280.195	298.504	616.672	660.111
1.8	0.6	0.25	166.038	171.209	149.434	148375	172.622	184.382	525.296	568.255
1.8	0.6	0.30	160.792	175.521	144.713	130.950	165.247	172.523	517.746	570.017

Experimental measurements were also performed that confirmed the analytical predictions with errors less than 6 percent. The corner-filleted flexures are shown to be more compliant in bending compared to the right circular flexures. They also induce substantially lower stresses but are less precise in keeping the position of the rotation center. All these conclusions are formulated after studying several compliance ratio functions that are defined in terms of two non-dimensional variables.

Nomenclature

A = flexure cross-sectional area, intermediate function
B = intermediate function
C = compliance
E = Young's modulus
F = force
I = Flexure cross-sectional moment of area, integral
K = stiffness
M = bending moment
N = normal force
U = elastic strain energy
b = flexure width
f = function
h = geometric variable
k = stress concentration factor
l = flexure length
r = fillet radius
t = flexure thickness
x, y, z = reference axes
$\delta, \varepsilon, \beta, \gamma$ = non-dimensional parameters
θ = rotation angle
σ = normal stress

Subscripts

a = axial
b = bending
e = elastic
min, max = minimum, maximum
x, y, z = reference axes

Superscripts

$*$ = right circular flexure hinge

9 Appendix

9.1 Moments of Area. The moment of area I varies since the cross-sectional thickness t is different on the three intervals, (1-2), (2-3) and (3-4) of Fig. 4. The thickness is expressed, respectively, as:

$$\begin{cases} t(x)=t+2[r-x^{1/2}(2r-x)^{1/2}], & x\in[0,r] \\ t(x)=t, & x\in[r,l-r] \\ t(x)=t+2[r-(l-x)^{1/2}(2r-l+x)^{1/2}, & x\in[l-r,l] \end{cases} \tag{48}$$

9.2 Bending Moment and Axial Force for Compliance Factors. Referring to Fig. 5, the bending moment and axial force of Eqs. (2) are:

$$\begin{cases} M=M_{z1}-xF_{y1} \\ N=F_{x1} \end{cases} \tag{49}$$

9.3 Bending Moment and Axial Force for Precision of Rotation. Referring to Fig. 5, the bending moment and axial force of Eqs. (2) are:

$$\begin{cases} M=M_{z1}-xF_{y1}+(x-l/2)F_{y5} \\ N=F_{x1}+F_{x5} \end{cases} \tag{50}$$

References

[1] Paros, J. M., and Weisbord, L., 1965, ''How to Design Flexure Hinges,'' Mach. Des., Nov., **25**, pp. 151–156.
[2] Ragulskis, K. M., Arutunian, M. G., Kochikian, A. V., and Pogosian, M. Z., 1989, ''A Study of Fillet Type Flexure Hinges and their Optimal Design,'' Vibration Engineering, **3**, pp. 447–452.
[3] Smith, T. S., Badami, V. G., Dale, J. S., and Xu, Y., 1997, ''Elliptical Flexure Hinges,'' Rev. Sci. Instrum., **68**, No. 3, pp. 1474–1483.
[4] Xu, W., and King, T. G., 1996, ''Flexure Hinges for Piezo-Actuator Displacement Amplifiers: Flexibility, Accuracy and Stress Considerations,'' Precis. Eng., **19**, No. 1, pp. 4–10.
[5] Weinstein, J. M., 1965, ''Flexure Pivot Bearings,'' Mach. Des., June 10, pp. 150–157.
[6] Goldfarb, M., and Speich, J. E., 1999, ''A Well-Behaved Revolute Joint for Compliant Mechanism Design,'' ASME J. Mech. Des., **121**, No. 3, pp. 424–429.
[7] Lobontiu, N., 2001, ''Distributed-Parameter Dynamic Model and Optimized Design of a Double Pendulum with Flexure Hinges,'' Mech. Mach. Theory, **36**, No. 5, pp. 653–669.
[8] Her, I., and Chang, J. C., 1994, ''Linear Scheme for the Displacement Analysis of Micropositioning Stages with Flexure Hinges,'' ASME J. Mech. Des., **116**, No. 3, pp. 770–776.
[9] Howell, L. L., and Midha, A., 1994, ''A Method for the Design of Compliant Mechanisms with Small-Length Flexural Pivots,'' ASME J. Mech. Des., **116**, No. 1, pp. 280–290.
[10] Ryu, J. W., Gweon, D.-G., and Moon, K. S., 1997, ''Optimal Design of a Flexure Hinge Based XY Wafer Stage,'' Precis. Eng., **21**, pp. 18–28.
[11] Ryu, J. W., and Gweon, D.-G., 1997, ''Error Analysis of a Flexure Hinge Mechanism Induced by Machining Imperfection,'' Precis. Eng., **21**, pp. 83–89.
[12] Ryu, J. W., Lee, S. Q., Gweon, D.-G., and Moon, K. S., 1999, ''Inverse Kinematic Modeling of a Coupled Flexure Hinge Mechanism,'' Mechatronics, **9**, pp. 657–674.
[13] Young, W. C., 1987, *Roark's Formulas for Stress and Strain*, McGraw Hill, New York.
[14] Peterson, R. E., 1974, *Stress Concentration Factors*, John Wiley and Sons, New York.